Available online at www.sciencedirect.com
SCIENCE DIRECT®
Computers and Geotechnics 32 (2005) 340–357
COMPUTERS AND GEOTECHNICS
www.elsevier.com/locate/compgeo

A novel discrete model for granular material incorporating rolling resistance

M.J. Jiang [a,b,*], H.-S. Yu [a], D. Harris [b]

[a] Nottingham Centre for Geomechanics, School of Civil Engineering, University of Nottingham, University Park, Nottingham NG7 2RD, UK
[b] School of Mathematics, University of Manchester, P.O. Box 88, Manchester M60 1QD, UK

Received 13 September 2004; received in revised form 17 March 2005; accepted 10 May 2005
Available online 1 July 2005

Abstract

This paper presents a novel two-dimensional (2D) discrete model for granular materials with rolling resistance. The salient features of our formulation are: it consists of a geometrically derived kinematical model, physically based mechanical contact models and locally equilibrated equations governing the motion of the rigid particles; only one additional parameter δ needs to be introduced in the model when compared with the standard discrete element method (DEM). In the study, precise definitions of pure sliding and pure rolling were proposed, and a decomposition of a general contact displacement was given in terms of these rolling and sliding components which are then linked to energy dissipation. The standard DEM assumption that grains are in contact at discrete points was here replaced by the assumption that grains are in contact over a width. By making the idealization that the grain contact width is continuously distributed with normal/tangential basic elements, we established a rolling contact model together with normal/tangential contact models, and also related the governing equations to local equilibrium. As an example of its application, the present model was incorporated into a DEM code to study the angle of internal friction ϕ of the material. Fifty-four DEM simulations showed that ϕ predicted by the novel model was increased in comparison to the standard DEM prediction, and may be closer to the values observed experimentally provided that the δ–ϕ relationship established in this paper was used.

Keywords: Kinematical models; Contact laws; Granulates; Rolling resistance; Discrete element methods

1. Introduction

Constitutive modelling of granular materials has attracted great interest amongst researchers and has a long history in geomechanics among which are several prefailure plasticity models [1–5] and several post-failure plasticity models [6–9]. These classical plasticity models are developed within the framework of classical continuum mechanics, in which *particle rotations* and grain length scale of granular materials are not emphasized. Several theories were proposed which introduce only a microstructural length scale into the constitutive models for granular materials [10–13]. However, their physical assumptions have not yet been well investigated due to lack of experimental data. For example, the theoretical assumption of micro-polar theory [10,11] was only investigated numerically by the standard discrete element method (DEM) [14,15], in which *particle rotation* is assumed to be either free or strictly prevented [16], i.e., particle rotations are controlled by the moments solely resulting from tangential contact forces at particle contacts or suppressed to be zero in the simulations.

Particle rotation has been found very important in controlling the behaviour of granular materials. For example, it is reported that *interparticle rolling* dominates as a microscale mechanism in controlling peak strength of granular materials [17], and leading to extensive dilatancy of granular media [18]. Particle rotation

* Corresponding author. Tel.: +44 115 951 3988; fax: +44 115 951 3898.
E-mail address: mingjing.jiang@nottingham.ac.uk (M.J. Jiang).

0266-352X/$ - see front matter © 2005 Elsevier Ltd. All rights reserved.
doi:10.1016/j.compgeo.2005.05.001

has been also regarded as an important factor in elastic micro-mechanical models [19–21]. Because of the great difficulty in measuring particle rotation in the geo-laboratory even with such advanced techniques as the stereo-photogrammetric technique [22] and particle image velocimetry (PIV) [23], particle rotation is neither fully understood in micro-mechanics nor adequately linked to macro-constitutive modelling of granular materials, see [24,25]. Hence, the DEM proposed by Cundall and Strack [14,15] has been widely accepted as a useful alternative tool in studying particle rotation. There are two main approaches for the contact constitutive relations to investigating particle rotation. The first is to measure the rotation field within an assembly of granular material, and then compare it with the continuum spin of the assembly [26–31], using standard DEMs [14,15], in which particle rotation is assumed to be either free or strictly prevented. Now, numerous research papers have shown that the free particle rotation in an assembly leads to a reduced aggregate frictional behaviour in numerical simulations [32–35]. The assemblies also develop a microstructure different from that observed in experiments in natural sands [36]. This discrepancy attributes to the large amount of rolling and has led to several researchers to implement other shaped particles to inhibit particle rolling in order to increase strength values, and hence produce more realistic behaviour [33,37–43]. It is also difficult to find either a physical or mechanical basis of strictly preventing particle rotation in an assembly. The second approach is to establish contact laws related to particle rotation, and to take into account *rolling resistance* at the particle contacts.

By *rolling resistance* we mean that a couple may be transferred between the grains via the contacts, and this couple resists particle rotations. There is physical evidence for the existence of rolling resistance. For example, real grains may exhibit a rough surface texture, and may even be covered with a thin film of weathered products [44]. In this case the grains may be in contact with their neighbours through contact surfaces so that rolling resistance may have an effect on the mechanical behaviour of the granular material. Rolling resistance may, analytically and experimentally, exist even at contacts between cylindrical grains [45]. In addition, several researchers have stated the importance of rolling resistance in DEM simulations of granular material, such as in elastic micro-mechanical model [19], sand pile [46] and granular flow [47] simulations. In geomechanics, Iwashita and Oda [48,49] found that not only the generation of large voids inside a shear band but also a high gradient of particle rotation along the shear band boundaries can be reproduced by their rolling resistance model in a manner similar to those observed in experiments on natural granular soils [43], which was found difficult to simulate using standard DEM. Their subsequent analysis emphasized the potential to study couple stresses in granular materials by DEM with rolling resistance [50].

The simulations by Iwashita and Oda [48,49] have confirmed the importance of a *rolling resistance model* to granular mechanics. These two papers [48,49] have been regarded as two of classical papers in granular mechanics. However, there appear to be several aspects of their model in need of further investigation, which will be explained separately in the next sections: (1) The kinematical model was stated for discs of equal radius in contact but without theoretical proof. (2) The rolling resistance model was introduced artificially with four additional model parameters, with three of them chosen separately by trial and error and fourth related to particle overlap in value. (3) The equations governing angular motion of particles were not linked to an underlying equilibrium configuration of the system.

The main objective of this paper is to present a mathematical model for a discrete granular material with rolling resistance, which can avoid the limitations in [48,49]. Firstly, new definitions of pure sliding and pure rolling are introduced in order to decompose displacements of contact into rolling and sliding components in a unique and general manner, which are then analysed in the light of energy dissipation. Secondly, a parameter, called the *shape parameter* δ, is proposed to represent the contact width between grains and which is assumed to be continuously distributed with normal/tangential basic elements (BE). (Each BE is composed of spring, dashpot, slider and divider in analogous manner to those used with standard DEM). This leads to a rolling contact model together with normal and tangential contact models. Thirdly, it is assumed that there exists an underlying equilibrium state for the system and we consider motions about this equilibrium state. We shall say that the equations that govern the motion of the grains are derived on the basis of local equilibrium. Finally, 54 biaxial compression tests are simulated to show the behaviour of granular materials incorporating the proposed model by a DEM developed by one of the authors. No attempt is to make in this paper to carry out DEM numerical simulations of shear band with the model.

2. Kinematical model of particles in contact

In this section, we shall introduce kinematics of particles in contact, relative particle rotation, rotation rates and their relationship to work-rate, in the presence of rolling resistance. We shall introduce them in formulae similar to those used by Iwashita and Oda [48,49]. This method is different from that in the literature [51,52] in which a contact deformation mode, a contact rolling mode and a model of rigid particles were proposed.

2.1. Kinematics of particles in contact

Consider a 2D assembly of rigid discs incrementally deformed under plane strain conditions. The motion of a rigid body may be decomposed into the motion of the centre of mass together with the motion about the centre of the mass. During a time step from t to $t + \mathrm{d}t$, two discs 1 and 2 with radii r_1 and r_2, respectively, are assumed to remain in contact k, Fig. 1. Let n_1^k and n_2^k denote two unit vectors at time t, which are normal and tangential to the common surface at the contact point c, respectively. In addition, at time t, let o_1, o_2 denote the disc centres, α^k denote the angle that o_1o_2 makes with the x-axis, and o_1c, o_2c be radii marked on the disc. At time $t + \mathrm{d}t$, let c' denote the current contact point, $\mathrm{d}\alpha$ denote the angle between $o_1'o_2'$ and o_1o_2. The arcs $\overline{c'c_1'}$, $\overline{c'c_2'}$, which represent the displacement of the contact point c on discs 1 and 2, are denoted by $\mathrm{d}a$, $\mathrm{d}b$ respectively. All angles are measured in radians. Let $\mathrm{d}\theta_1$ and $\mathrm{d}\theta_2$ denote the angle between o_1o_2 and $o_1'c_1'$, $o_2'c_2'$, respectively. By taking counter-clockwise rotation as positive, $\mathrm{d}\theta_2$ and $\mathrm{d}\alpha$ are positive but $\mathrm{d}\theta_1$ is negative in the case shown. $\mathrm{d}a$ and $\mathrm{d}b$ can be related to the other variables [17,27,48]

$$\mathrm{d}a = r_1(\mathrm{d}\theta_1 - \mathrm{d}\alpha), \quad \mathrm{d}b = r_2(\mathrm{d}\theta_2 - \mathrm{d}\alpha), \tag{1a, b}$$

where $\mathrm{d}a$ and $\mathrm{d}b$ are positive when measured counter-clockwise, by following the convention for rotation. Thus $\mathrm{d}a$ is negative but $\mathrm{d}b$ is positive in the case shown in Fig. 1. However, the definitions of Eqs. (1) are valid for any disc displacements provided that the discs remain in contact during the time step from t to $t + \mathrm{d}t$.

Generally, $r_1 \neq r_2$, $\mathrm{d}a$ and $\mathrm{d}b$ are both composed of rolling and sliding components, denoted by $\mathrm{d}U_\mathrm{r}$ and $\mathrm{d}U_\mathrm{s}$, respectively. We now define two special types of contact displacement. A pure rolling displacement is defined by

$$\begin{cases} \mathrm{d}a = -\mathrm{d}b \neq 0, \\ \mathrm{d}U_\mathrm{s} = 0, \quad \mathrm{d}U_\mathrm{r} = \mathrm{d}a \end{cases} \tag{2a, b}$$

and a pure sliding displacement by

$$\begin{cases} \mathrm{d}a = \frac{r_1}{r_2}\mathrm{d}b, \quad \mathrm{d}a \neq 0 \text{ or } \mathrm{d}b \neq 0, \\ \mathrm{d}U_\mathrm{s} = \frac{\mathrm{d}a + \mathrm{d}b}{2}, \quad \mathrm{d}U_\mathrm{r} = 0. \end{cases} \tag{3a, b}$$

The definitions in Eqs. (2) and (3) differ from and are more proper than those used in [17,27,48]. Firstly, it can be seen that the pure rolling defined in [17,27,48], i.e., $\mathrm{d}a = -\mathrm{d}b$, is similar to Eq. (2a). However, Eq. (2a) excludes the special case where the two discs rotate together as a single rigid body (SRB). Secondly, three different definitions for pure sliding were used in [17,27,48], and each of them can be deduced from one part of the definition in Eqs. (3). For example, the pure sliding defined in [27], i.e., $\mathrm{d}a = \frac{r_1}{r_2}\mathrm{d}b$, is similar to Eq. (3a). But, Eq. (3a) has the advantage that the case of SRB is excluded. Similarly, pure sliding as defined by Iwashita and Oda [48], i.e., $\mathrm{d}a = \mathrm{d}b$, can be deduced from Eq. (3a) by choosing $r_1 = r_2$ and their paper ignores the possibility of SRB.

Based on Eqs. (2) and (3), $\mathrm{d}a$ and $\mathrm{d}b$ can be expressed uniquely as a linear combination of $\mathrm{d}U_\mathrm{r}$ and $\mathrm{d}U_\mathrm{s}$, respectively (see Appendix A)

$$\mathrm{d}a = \mathrm{d}U_\mathrm{r} + \frac{2r_1}{r_1 + r_2}\mathrm{d}U_\mathrm{s}, \quad \mathrm{d}b = -\mathrm{d}U_\mathrm{r} + \frac{2r_2}{r_1 + r_2}\mathrm{d}U_\mathrm{s}. \tag{4a, b}$$

Eqs. (4) are valid for a general contact displacement and give a unique decomposition in the kinematical analysis of contacting discs. The differing signs of $\mathrm{d}U_\mathrm{r}$ in Eqs. (4a,b) are a consequence of our analysis, and demonstrate the fact that the rolling contact displacement $\mathrm{d}U_\mathrm{r}$ gives rise to differing signs for $\mathrm{d}a$ and $\mathrm{d}b$. From Eqs. (4), $\mathrm{d}U_\mathrm{r}$ and $\mathrm{d}U_\mathrm{s}$ can be expressed, respectively, in terms of $\mathrm{d}a$ and $\mathrm{d}b$

$$\mathrm{d}U_\mathrm{r} = \frac{r_2\mathrm{d}a - r_1\mathrm{d}b}{r_1 + r_2}, \quad \mathrm{d}U_\mathrm{s} = \frac{\mathrm{d}a + \mathrm{d}b}{2}, \tag{5a, b}$$

which show consistency with our definitions of pure sliding and pure rolling. For two discs of equal radius, $r_1 = r_2$, Eqs. (4) and (5) become

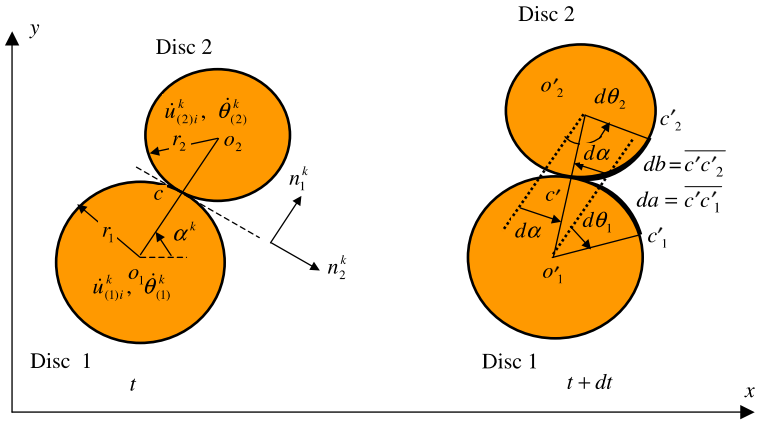

Fig. 1. Kinematics of discs in contact k at times t and $t + \mathrm{d}t$.

$$\mathrm{d}a = \mathrm{d}U_\mathrm{r} + \mathrm{d}U_\mathrm{s}, \quad \mathrm{d}b = -\mathrm{d}U_\mathrm{r} + \mathrm{d}U_\mathrm{s}, \tag{6a, b}$$

$$\mathrm{d}U_\mathrm{r} = \frac{\mathrm{d}a - \mathrm{d}b}{2}, \quad \mathrm{d}U_\mathrm{s} = \frac{\mathrm{d}a + \mathrm{d}b}{2}. \tag{7a, b}$$

Eqs. (6) and (7) are of the same form as those used by Iwashita and Oda [48] in their kinematical analysis of two discs in contact. This indicates that the decomposition formulae used in [48] are correct, although no proof is given there, but their formulae should be regarded as a special case of the general case presented in this paper.

Hence, $\mathrm{d}U_\mathrm{r}$ and $\mathrm{d}U_\mathrm{s}$, together with $\mathrm{d}U_n$ which is the relative displacement along the contact normal n_1^k, may be regarded as the three basic quantities which describe the kinematics at contact. We now derive a relationship between $\mathrm{d}U_\mathrm{r}$ and relative particle rotation.

2.2. Relative particle rotation

Relative particle rotation may be expressed in terms of particle displacements and rotations by the methods proposed by other searchers, e.g. [51,52]. We shall still introduce it in a manner similar to that used by Iwashita and Oda [47,48]. For simplicity, consider that two discs, 1 and 2 with radii r_1 and r_2, experience a pure rolling during a time interval from t to $t + \mathrm{d}t$, as shown in Fig. 2, while the disc centres o_1, o_2 are fixed. Let l_1l_2 be the common tangent plane at the contact point c. Let c_1, c_2 be the points on the surface of discs 1 and 2, respectively, at time t, which will coincide at the common contact c at time $t + \mathrm{d}t$. o_1c_1, o_2c_2 are the radii marked on the discs. After the incremental time $\mathrm{d}t$, the arcs $\overline{cd_1}$, $\overline{cd_2}$ represent the displacement of the contact point c on discs 1 and 2, respectively, with $|\overline{cd_1}| = |\overline{cd_2}|$. Thus the lines o_1c_1, o_2c_2, o_1c and o_2c at time t arrive, respectively, at o_1c, o_2c, o_1d_1 and o_2d_2 at time $t + \mathrm{d}t$. Likewise, the lines c_1c and c_2c at time t, arrive at cd_1 and cd_2, respectively, at time $t + \mathrm{d}t$. Denote by $\mathrm{d}\theta_1$ and $\mathrm{d}\theta_2$ the angle between o_1o_2 and o_1d_1, o_2d_2, respectively. Again, taking counter-clockwise rotation as positive, $\mathrm{d}\theta_1$ is positive but $\mathrm{d}\theta_2$ is negative in the case shown in Fig. 2.

In the next section we shall require an expression for the length of c_1c (c_2c) in the micro-mechanical contact

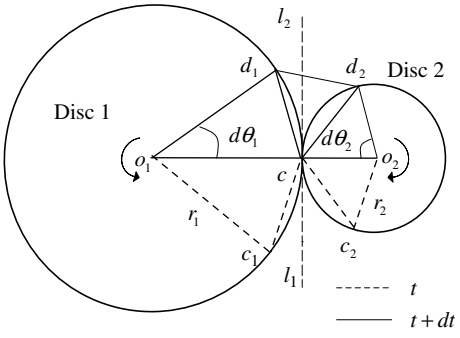

Fig. 2. Pure rolling in contact k at times t and $t + \mathrm{d}t$: ($\mathrm{d}\theta_r = \mathrm{d}\theta_{c_1c} - \mathrm{d}\theta_{c_2c} = \angle c_1cl_1 + \angle d_1cl_2 - (\angle c_2cl_1 + \angle d_2cl_2)$).

model, hence it is convenient here to define a *relative particle rotation* $\mathrm{d}\theta_\mathrm{r}$ physically as the angle change between line c_1c and c_2c. Following the sign convention of rotation in this paper, $\mathrm{d}\theta_\mathrm{r}$ can be related to $\mathrm{d}U_\mathrm{r}$, r_1 and r_2 as follows:

$$\mathrm{d}\theta_\mathrm{r} = \mathrm{d}\theta_{c_1c} - \mathrm{d}\theta_{c_2c} = \frac{\mathrm{d}U_\mathrm{r}}{r_1} + \frac{\mathrm{d}U_\mathrm{r}}{r_2}, \tag{8}$$

where $\mathrm{d}\theta_{c_1c}$ is the angle subtended by c_1c and similarly for $\mathrm{d}\theta_{c_2c}$. This leads to

$$\mathrm{d}\theta_\mathrm{r} = 2\frac{\mathrm{d}U_\mathrm{r}}{r}, \tag{9a}$$

where the common radius r is defined by

$$r = \frac{2r_1r_2}{r_1 + r_2}. \tag{9b}$$

Although Eqs. (8) and (9) are derived from the physical definition of *relative particle rotation*, they can also be obtained from Eqs. (1) and (4) by defining *the relative particle rotation* as $\mathrm{d}\theta_\mathrm{r} = \mathrm{d}\theta_1 - \mathrm{d}\theta_2$ as used in [17]. Thus, using either definition, Eqs. (9) can be regarded as a general formula relating $\mathrm{d}\theta_\mathrm{r}$ with $\mathrm{d}U_\mathrm{r}$. Eqs. (8) and (9) are different from and more proper than those used by Iwashita and Oda [48]. For example, in their DEM analyses, the following equations were used without any theoretical proof:

$$\mathrm{d}\theta_\mathrm{r} = \frac{\mathrm{d}U_\mathrm{r}}{r'}, \quad r' = (r_1 + r_2)/2. \tag{10a, b}$$

Eqs. (10a) are similar, but not identical, in form to Eq. (9a) but Eq. (10b) is different from Eq. (9b). Hence, Eqs. (8) and (9), which have been given a rigorous derivation above, are different from and more proper than the corresponding equations used in [48]. Eqs. (8) or (9) can be expressed in a rate form, to be introduced in the next subsection.

Note that if we choose $r_2 \to \infty$, as for a disc-wall contact, Eqs. (8) or (9) become

$$\mathrm{d}\theta_\mathrm{r} = \frac{\mathrm{d}U_\mathrm{r}}{r_1} = \frac{2\mathrm{d}U_\mathrm{r}}{r}, \quad r = 2r_1 \tag{11a, b}$$

which is of the same form as Eq. (9a) and hence our formula may be used for both particle–particle and wall–particle contacts. However, it should be noted that Eq. (10) used in [48] is not of the same form as Eq. (11) and so cannot be used for particle–wall contacts, another limitation in [48].

2.3. Rotation rates

We shall propose three different rotation rates in this subsection, two of which are to related to the work rate in the next subsection. Using Eqs. (1), (5a) and (9), $\mathrm{d}\theta_\mathrm{r}$ can be then derived in terms of particle rotations

$$\mathrm{d}\theta_\mathrm{r} = \mathrm{d}\theta_1 - \mathrm{d}\theta_2. \tag{12}$$

By dividing both sides of Eq. (12) with incremental time dt, the first rotation rate, called the *relative rotation rate* $\dot{\theta}_r$, can be obtained

$$\dot{\theta}_r = \frac{d\theta_r}{dt} = \frac{d\theta_1}{dt} - \frac{d\theta_2}{dt} = \dot{\theta}_1 - \dot{\theta}_2. \tag{13}$$

Eqs. (12) and (13) are very important in establishing contact models and DEM numerical analyses in next sections. Since dU_s is associated physically with energy dissipation as defined in classical continuum mechanics, a quantity, which is here called *sliding rotation* $d\theta^s$, may be defined in a manner similar to Eq. (9a)

$$d\theta^s = 2\frac{dU_s}{r}, \tag{14}$$

where r is defined in Eq. (9b).

Using Eqs. (1) and (7b), $d\theta^s$ can be rewritten as follows:

$$d\theta^s = \frac{(r_1 + r_2)}{2}\left[\left(\frac{d\theta_1}{r_2} + \frac{d\theta_2}{r_1}\right) - \left(\frac{d\alpha}{r_2} + \frac{d\alpha}{r_1}\right)\right]. \tag{15}$$

By dividing Eq. (15) with dt and taking the limit as $dt \to 0$, we obtain the second rotation rate, called the *sliding rotation rate* $\dot{\theta}^s$,

$$\dot{\theta}^s = \frac{d\theta^s}{dt} = \frac{1}{r}\left[r_1\dot{\theta}_1 + r_2\dot{\theta}_2 - (r_1 + r_2)\dot{\alpha}\right]. \tag{16}$$

The third rotation rate, *pure rotation rate* $\dot{\theta}^p$, is defined as follows:

$$\dot{\theta}^p = \frac{1}{r}\left(r_1\dot{\theta}_1 + r_2\dot{\theta}_2\right). \tag{17}$$

Eq. (16) leads to

$$\dot{\theta}^s = \dot{\theta}^p - \frac{1}{r}(r_1 + r_2)\dot{\alpha}. \tag{18}$$

If the two discs are of equal radii, Eqs. (17) and (18) become, respectively,

$$\dot{\theta}^p = (\dot{\theta}_1 + \dot{\theta}_2), \quad \dot{\theta}^s = \dot{\theta}^p - 2\dot{\alpha}. \tag{19a, b}$$

Eq. (18) or (19b) shows that the energy dissipation-related $\dot{\theta}^s$ has terms containing both $\dot{\theta}^p$ and $\dot{\alpha}$. The first term is described in terms of the rotation of particles while the second part in terms of the motion of grain centres. However, the motion and deformation of bodies in classical continuum mechanics is defined solely in terms of velocity and/or displacement, see e.g. [53], and is represented here by $\dot{\alpha}$. This leads to the fact that $\dot{\theta}^p$ is neglected in classical continuum mechanics and consequently in continuum models. It appears to be necessary to include $\dot{\theta}^p$ in continuum models for granular materials, such by an averaged way in [54]. In addition, it has been pointed out by several authors, e.g. [32], that rolling resistance has been neglected from the contact law mechanics in standard DEM [14,15]. In this study on a discrete model, we will focus attention on $\dot{\theta}_r$ and demonstrate in the next subsection its role in the work-rate for granular materials.

2.4. Work-rate

Since grains are considered to be rigid discs, work done by the normal component contact force is elastic and hence recoverable and is not considered. In addition, we will assume the existence of a couple at a contact. The mechanical model underlying this idea is introduced in the next section. As a general case, suppose that, during a time interval from t to $t + dt$, the tangential contact force at the contact k and the couple about the contact k change linearly from F_s^k and M^k to $(F_s^k + dF_s^k)$ and $(M^k + dM^k)$, respectively. In the time interval dt, the displacement of the contact point c on discs 1 and 2 is denoted by da, db, respectively (see Fig. 1). In the interval dt, using the definition of work in classical mechanics, the incremental work dW^k by the force and couple on the two discs done at contact k by the tangential force and the couple may be written as

$$dW^k = \frac{(2F_s^k + dF_s^k)\,da}{2} + \frac{(2F_s^k + dF_s^k)\,db}{2m_1} + \frac{(2M^k + dM^k)\,da}{2r_1} + \frac{(2M^k + dM^k)\,db}{2r_2m_2}, \tag{20}$$

where m_1, m_2 may be +1 or −1 and its sign needs to be decided by further analysis.

Eq. (20) is a general formula of the incremental work done by the contact force and couple at the contact and governs the amount of energy dissipation in granular materials when plastic sliding or rolling occurs at the contact. Furthermore, Eq. (20) can be expressed specifically as follows (see Appendix B):

$$dW^k = \frac{(2F_s^k + dF_s^k)(da + db)}{2} + (2M^k + dM^k)\left(\frac{da}{2r_1} - \frac{db}{2r_2}\right). \tag{21}$$

By using Eqs. (1) and (8), Eq. (21) can be rewritten as

$$dW^k = (2F_s^k + dF_s^k)dU_s + (2M^k + dM^k)\,\frac{d\theta_r}{2}, \tag{22}$$

where *relative particle rotation* $d\theta_r$ is defined in Eqs. (9).

Eq. (22) indicates that dW^k can be decomposed into a sum of two terms. The first term is related to dU_s via the tangential contact force. The second term is related to $d\theta_r$ via the couple at the contact. Evidently, if the couple at the contact is identically zero, the second term in the expression for the incremental work is also zero.

Using Eqs. (13), (14) and (16), and dividing the both sides of Eq. (22) with dt and taking the limit as $dt \to 0$, the work rate $\dot{W}^k$ at time t can be related to the *sliding rotation rate* $\dot{\theta}^s$ and the *relative rotation rate* $\dot{\theta}_r$ by

$$\dot{W}^k = F_s^k r\dot{\theta}_s + M^k\dot{\theta}_r = M_s^k\dot{\theta}_s + M^k\dot{\theta}_r, \quad M_s^k = F_s^k r. \tag{23a, b}$$

Eq. (23b) is the moment due to the tangential contact force about the disc centre. Eqs. (23) demonstrate that $\dot{\theta}_r$ plays an important role in the energy dissipation of granular materials in the case where there is a couple/rolling resistance at contact, i.e., $M^k \neq 0$. Note that the work rate is expressed for contact k. The total work rate of an assembly may be obtained by accumulating the work rate over all contacts in the whole assembly by using a method similar to that proposed by [55] and is omitted here. In the next section we shall consider how to incorporate into $\dot{\theta}_r$ contact models for granular materials with rolling resistance.

3. Contact models for granular materials with rolling resistance

3.1. Physical model incorporating rolling resistance

We shall consider a general case in which the work component associated with $\dot{\theta}_r$ is non-zero, and that the inter-granular forces are composed only of contact forces, all other forces, for example van der Waals forces, are excluded from consideration. In this case, the rolling resistance is zero when grains are in contact with their neighbours at a single point. Thus a contact couple may only be transferred from one grain to another when they are in contact over an area, and we shall refer to such a contact of grains as a contact surface. For simplicity, we consider two rigid discs, 1 and 2 with radii r_1 and r_2, that are in contact over a width B defined as follows:

$$B = \delta \cdot r, \tag{24}$$

where the quantity δ is a dimensionless material and geometrical parameter which will generally be related to grain shape, and which we shall call the *shape parameter*. Eq. (24) naturally leads to that: given a δ, contact width is proportional to particle sizes; and given a particle size (contact width), δ is proportional (inverse) to contact width (particle sizes). A realistic physical setting of δ needs further micro-experimental investigation into grain shapes, and will not be discussed in this study. However, as will be discussed in Section 5, δ can be properly chosen by comparing the angle of internal friction of the assembly to a targeted experimental data. Given a fixed value of δ, the corresponding value of B is solely dependent upon the value of r, where r is defined by Eq. (9b). This definition differs from and seems better than that used by Iwashita and Oda [48,49], in which their quantity B is a variable 'depending on such factors as normal force, normal stiffness value and grain size'. There are two points worthy of noting about the definition in Eq. (24). Firstly, as can be shown below, it will lead to our discrete model incorporating physically rolling resistance in a very simple formulation. Secondly, it naturally relates the difference of shear strength due to B to grain shape, which is in agreement with the knowledge in granular mechanics, e.g. [38,39].

We define a normal basic element (BE) at a point of contact to consist of a spring and dashpot in parallel together with a divider in series, see Fig. 3. Similarly, a tangential BE consists of a spring and dashpot in parallel together with a slider in series. We here propose a micro-mechanical model in which there is a contact width and on which is a continuously distributed system of *normal and tangential* BEs. Clearly, the normal BEs contribute to the rolling resistance at the contact surface, while the tangential BEs do not. We shall take the distributed normal BEs (which involve only the normal component of the contact force) to constitute a normal micro-mechanical model for the rolling resistance, and this is illustrated in Fig. 3. In Fig. 3, each normal BE includes a spring with stiffness as k_n (in N/m^2) reflecting an elastic behaviour, a dashpot with damping parameter η_n (in s Pa) allowing energy dissipation, and a divider to simulate the fact that traction force (in N/m) is not transmitted through a BE at a point where the grains are not in contact at that point. We call this a point-divider. The tangential micro-mechanical model is analogous to the normal micro-mechanical model except

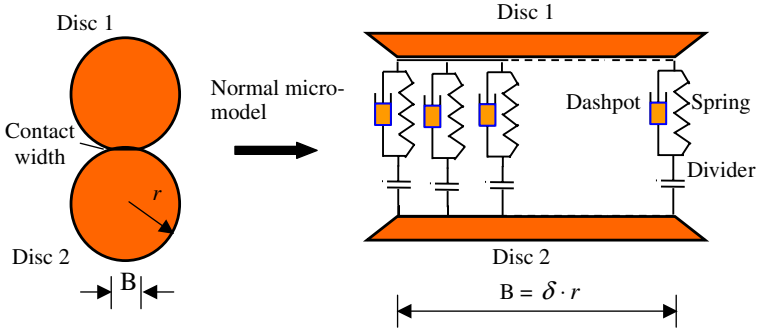

Fig. 3. Normal micro-mechanical model for rolling resistance at contact.

that the springs and dashpots are tangential and a tangential slider replaces the divider in each BE. The slider simulates plastic sliding at the point, with a point-shear strength (in N/m) of magnitude equal to that associated with the given normal force (in N/m) and defined by Mohr–Coulomb criterion. Denote by K_n and K_s (in N/m) the resultant normal and tangential stiffness, respectively, for the BEs, and denote by μ_n (in s N/m) the resultant damping parameter of the normal dashpot. Also, let k_n (k_s) denote the normal (tangential) stiffness of each BE, respectively, and satisfy:

$$K_n = k_n B, \quad K_s = k_s B, \quad \mu_n = \eta_n B. \tag{25a, b, c}$$

We use the same concept of *relative particle rotation* $\mathrm{d}\theta_r$ as defined in Eq. (9), but here consider a finite relative rotation, which we shall denote by θ_r, and let B represent c_1c or c_2c in Fig. 2. Then, if there is relative particle rotation, a couple will result at the contact and be transferred from one grain to the other. We shall derive the relationship between the couple M and θ_r in the case of small θ_r. We shall establish a physical model for M in three steps. Firstly, consider the case that none of the dividers are separated, which we shall see corresponds to linear elastic case. Secondly, turn to the case that some dividers are separated, which we shall associate with the plastic case. Finally, we shall establish simplified rolling resistance models.

Firstly, let us consider a contact where none of the dividers are separated, see Fig. 4. When grain 1 rotates counter-clockwise through an angle θ_r against grain 2 under a fixed total normal contact force F_n, the normal

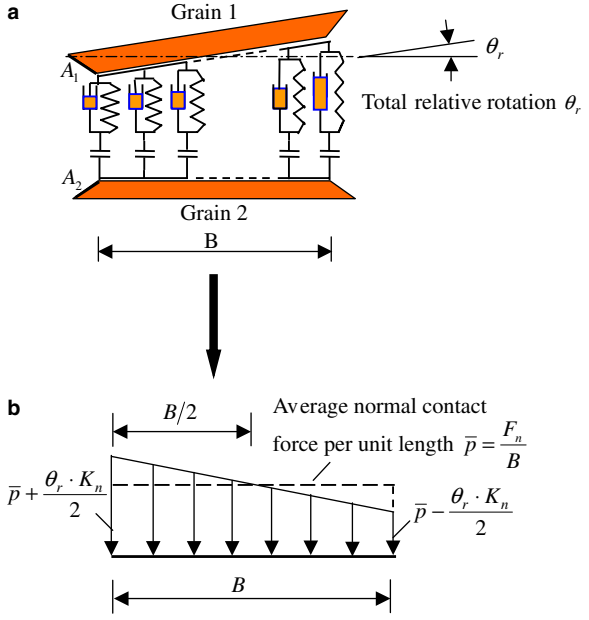

Fig. 4. Distribution of normal contact stress without dividers separated.

contact force per unit length p along the contact is distributed linearly as illustrated in Fig. 4(b). Then p at the right-hand side (p^r) and at the left-hand side (p^l) of the contact can be calculated, respectively, by

$$p^l = \bar{p} + \frac{\theta_r \cdot K_n}{2}, \quad p^r = \bar{p} - \frac{\theta_r \cdot K_n}{2}, \tag{26a, b}$$

where the average normal contact force per unit length $\bar{p}$ is calculated by

$$\bar{p} = \frac{F_n}{B}. \tag{27}$$

The distribution of p shown in Fig. 4(b) leads to the following expression for M at the contact:

$$M = \frac{\theta_r \cdot K_n \cdot B^2}{12} = K_m \theta_r, \tag{28}$$

where K_m is the *rolling stiffness* (in N m), following the term used by Iwashita and Oda [48,49]. Thus,

$$K_m = \frac{K_n \cdot B^2}{12} = \frac{K_n \cdot r^2}{12}\delta^2. \tag{29}$$

Eq. (28) indicates that M increases linearly with total *relative particle rotation* θ_r with the constant of proportionality K_m and $\theta_r = 0$ corresponds to $M = 0$. In addition, the condition $B = 0$ gives to $K_m = 0$, which then results in $M \equiv 0$. The *rolling stiffness* K_m is a constant here depending on the *shape parameter* δ, the common radius r and the normal stiffness K_n used in standard DEMs [14,15]. $\delta = 0$ corresponds to $K_m = 0$. However, in the rolling resistance model used in [48,49] K_m was an independent parameter and must be determined by trial and error and this is evidently not proper than Eq. (29) here. Eq. (28) represents an linear elastic rolling resistance response. We now turn to the case of plastic response. We shall define the plastic mechanism as the separation of the dividers.

Secondly, let us consider a contact in which some dividers are separated, see Fig. 5. When grain 1 rotates counter-clockwise against grain 2 under a fixed F_n, separation first occurs at the divider of the BE at the right-hand edge of the contact, as shown Fig. 5(a). With increasing θ_r, the point separation moves continuously inward from the right-hand edge, giving a zero value of p at the corresponding point. Consequently, p will be re-distributed linearly, as illustrated in Fig. 5(b). Denote by l the contact width that is still distributed with the remaining in-contact dividers. The minimum (maximum) normal contact stress at the right (left)-hand edge of the width l, denoted by $p_{\min}$ ($p_{\max}$), can be calculated by

$$p_{\min} = 0, \quad p_{\max} = \frac{l \cdot \theta_r \cdot K_n}{B}. \tag{30a, b}$$

Hence, M and F_n at the contact can then be obtained as follows:

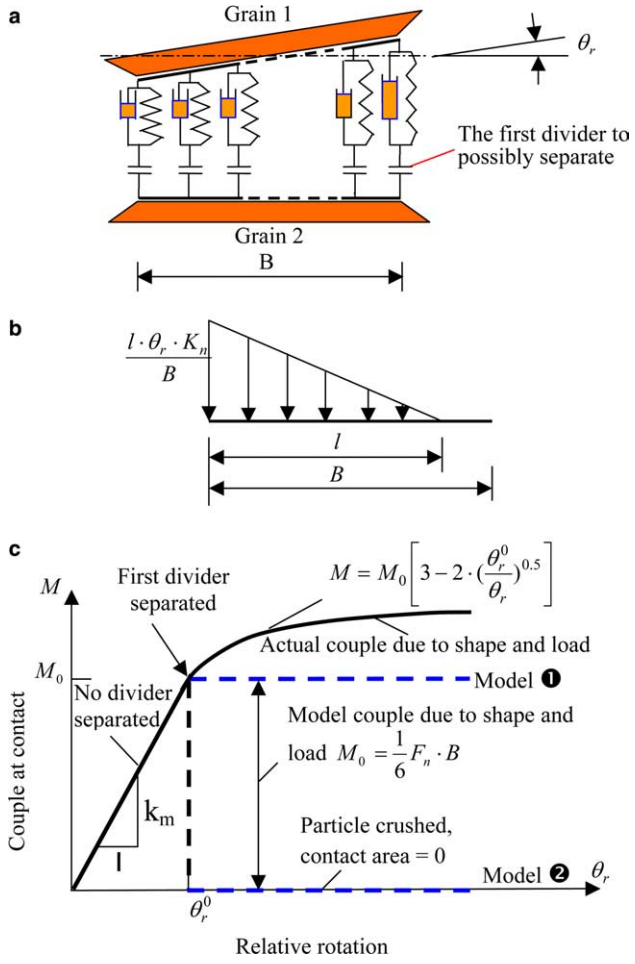

Fig. 5. Sketch for the rolling contact models with some separation of dividers. (a) Separation mechanism due to relative rotation at contact. (b) Distribution of normal contact force per unit length after some separation of dividers. (c) Rolling contact models.

$$M = \frac{\theta_r \cdot K_n \cdot l^2}{2B}\left(\frac{B}{2}-\frac{l}{3}\right), \quad F_n = \frac{\theta_r \cdot K_n \cdot l^2}{2B}. \tag{31a, b}$$

From Eqs. (31), we obtain

$$M = (F_n \cdot B)\left(\frac{1}{2}-\frac{l}{3B}\right), \quad l = \left(\frac{2F_nB}{K_n\theta_r}\right)^{0.5}. \tag{32a, b}$$

Let θ_r^0 and M_0 denote the critical values of θ_r and M, respectively, at $l = B$, which separate the elastic from the plastic case. Then, Eqs. (32) lead to

$$M_0 = \frac{1}{6}(F_n \cdot B), \quad \theta_r^0 = \frac{2F_n}{K_nB}. \tag{33a, b}$$

Substituting Eqs. (33) into Eqs. (32), the rolling resistance at $l \leqslant B$ can be expressed by

$$M = M_0\left[3-2\cdot\left(\frac{\theta_r^0}{\theta_r}\right)^{0.5}\right]. \tag{34}$$

Eq. (34) shows that, with a given M_0, M increases non-linearly with θ_r to a limit value of $3M_0$ after some separation of dividers. Eqs. (28) and (34) constitute the *rolling contact model* or *rolling resistance model* and has been derived from our micro-mechanical model.

Finally, we turn to an idealization of the rolling resistance model. As shown by the black curve in Fig. 5(c), the rolling contact model consists of an initial linear part controlled by Eq. (28), followed by a non-linear part described by Eq. (34). The nonlinearity leads to an additional difficulty in both theoretical and numerical analyses. Thus, two idealized rolling contact models are proposed here as follows:

(a) Elasto-perfectly plastic model – Model 1

$$\begin{cases} M = K_m\theta_r = \frac{\theta_r \cdot K_n \cdot B^2}{12}, & \theta_r \leqslant \theta_r^0, \\ M = M_0 = \frac{1}{6}(F_n \cdot B), & \theta_r > \theta_r^0. \end{cases} \tag{35a, b}$$

(b) Elasto-brittle-plastic model – Model 2

$$\begin{cases} M = K_m\theta_r = \frac{\theta_r \cdot K_n \cdot B^2}{12}, & \theta_r \leqslant \theta_r^0, \\ M = 0, & \theta_r > \theta_r^0. \end{cases} \tag{36a, b}$$

Eqs. (35) and (36) may be called *simplified rolling or resistance contact models*. Note that both simplified models reduce to a standard DEM by choosing $\delta = 0$. Models 1 and 2 are illustrated by the dotted lines, respectively, in Fig. 5(c). Model 1 is an approximation to the rolling resistance model, and shows elasto-plastic behaviour with a failure criterion similar to the Mohr–Coulomb criterion. In form, this model is similar to that used by Iwashita and Oda [48,49]. However, the two approaches are in essence different. For example, they treated K_m as an independent parameter to be determined by trial and error, while here K_m depends solely on K_n, δ and r. They used another empirical parameter $\alpha = 0$–6 to determine peak rolling resistance through $M_0 = \alpha BF_n$, although they emphasized that 'α should physically be less than one if cohessionless particles with a circular cross-section are only considered'. In the model here, M_0 is decided through Eq. (35b), which leads to $\alpha = \frac{1}{6}$ in their model. Hence, our model here can avoid the empiricism in their model. Model 2 proposed can be interpreted as a model for a type of idealized '*crushable* grain, where crushability is assumed to be described by the *abrupt disappearance of contact width* and which leads to the *abrupt loss of rolling resistance*. Model 2 is different from those models for grain crushing in the DEM analysis by McDowell and Harireche [56], where grain crushing was interpreted as the breakage of whole grain into lots of smaller grains. Model 2 can find also its experimental evidence in geotechnical engineering since the shape of granular materials used in high rock-fill dams becomes 'rounder' after construction,

which may be regarded as a kind of crushability [57]. With the aim of an application of the model to DEM, we shall introduce a mechanical contact model for the normal, tangential and rolling directions in the next subsection.

3.2. Mechanical contact models

Based on the micro-mechanical model proposed in the previous subsection, the continuously distributed tangential basic element (BE) can be incorporated directly into a total tangential contact model that controls the tangential behaviour at the contact. Meanwhile, the continuously distributed normal BE can be used to obtain a total normal contact model controlling the normal behaviour together with a rolling contact model controlling rolling behaviour at the contact. Consequently, the complete mechanical contact model is composed of normal, tangential and rolling contact components, as illustrated in Fig. 6: a normal contact model to resist normal force, a tangential contact model to resist shear force and a rolling contact model to resist rolling. These three components are similar in principle. They all include a spring reflecting elastic behaviour of the contact and a dashpot allowing energy dissipation and quasi-static deformations. The normal contact model includes a divider to simulate the fact that no force is transmitted when the grains are separated. The tangential contact model includes a slider that provides the contact shear resistance controlled by Mohr–Coulomb criterion. The rolling contact model includes a roller that represents the contact rolling resistance described by Eqs. (35) or (36).

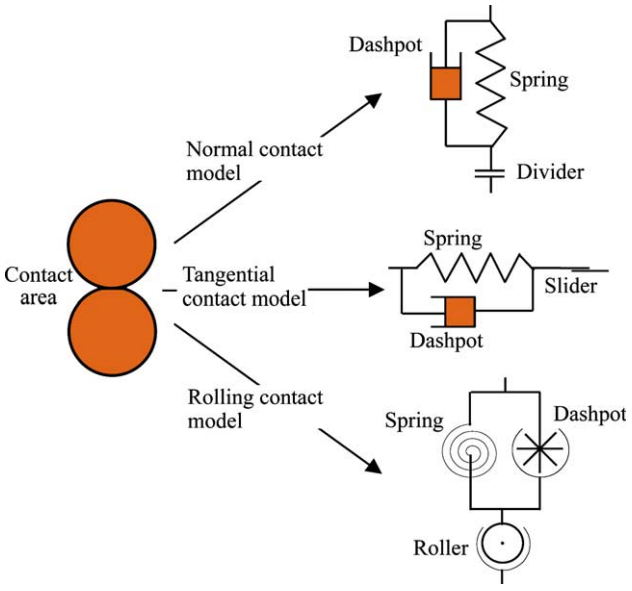

Fig. 6. The contact models proposed for grains with rolling resistance.

Fig. 7 presents the mechanical response of the normal, tangential and rolling contact models. The normal contact model is characterized by the stiffness parameter K_n (in N/m in a two-dimensional system). The tangential contact model is characterized by the stiffness parameter K_s; when plastic sliding occurs, the strength of the contact is maintained at a constant shear strength (in N) associated with the normal force (in N) and defined by the Mohr–Coulomb criterion. The rolling contact model is characterized by the stiffness parameter K_m (in N m in

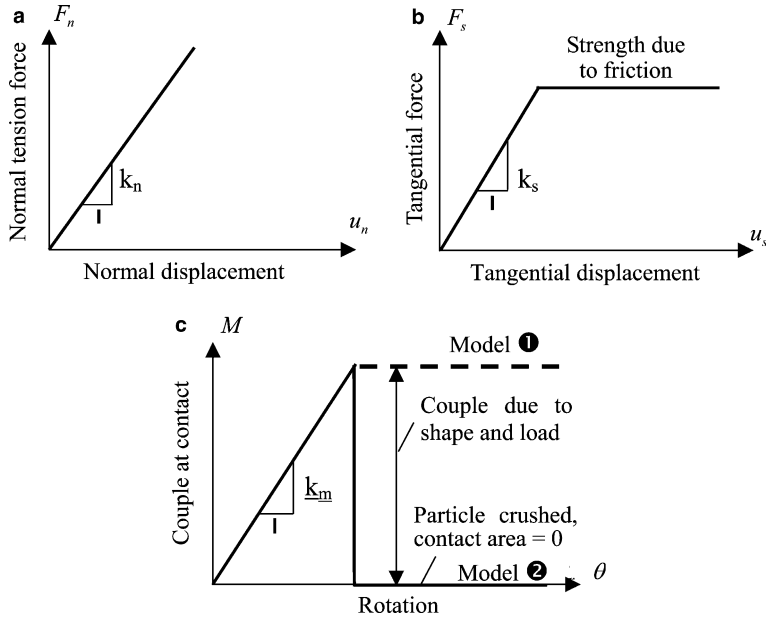

Fig. 7. Mechanical response of the contacts models: (a) normal contact model; (b) tangential contact model; (c) rolling contact model.

a two-dimensional system), which is dependent on K_n, the *shape parameter* δ and the common radius r; when the plastic rolling occurs, the rolling resistance (in N m) at the contact is maintained at a value defined by Mohr–Coulomb type criterion in Model 1 or abruptly reduces to zero in Model 2. Note that, although the derivation of the mechanical models appears to be complicated, their final expressions are in simple formulae and can be easily implemented in a DEM code.

We shall develop in the next section the equations governing the motion of grains with rolling resistance. These equations form one of the bases for DEM analysis.

4. Equations governing motions of grains with rolling resistance

In our micro-mechanical model, a grain contact is continuously distributed with normal/tangential basic element (BE), and only the normal BE contributes to the rolling resistance at the contact. It is clear that rolling resistance (couple) does affect the angular motion but not the translational motions of grains in a direct way. Hence, we shall consider a reduced problem in which a grain is in contact with a wall, and in which contact is continuously distributed with normal BE. We shall derive the governing equations based on a local equilibrium condition, which will be explained in detail below, in this reduced problem at first. Then, we shall develop the governing equations by considering a grain with several contacts in a general case, in which a grain contact is continuously distributed with normal/tangential BE.

4.1. Grain with a single contact in a reduced case

Fig. 8(a) shows the initial position of a particle in contact with a wall through a contact on which is continuously distributed with normal BE. The particle is stationary, and contact forces/couple are constant at the contact, at the position of *local equilibrium*. Consider a normal BE with arm length z from the X axis, and two sets of rectangular Cartesian coordinate axes OXY and $O'X'Y'$. $O'X'Y'$ are the coordinate axes fixed in the grain, with O' at the grain centre of mass and $O'Y'$ ($O'X'$) parallel (perpendicular) to the contact surface B_1B_2. The width of B_1B_2 is B as defined in Eq. (24). OXY are the coordinate axes fixed in space, they coincide with $O'X'Y'$ in the initial position. Assume that the grain experiences a displacement only in the X direction accompanied with a small rotation about the centre of mass, in the current position shown in Fig. 8(b). This leads to angular and translational motion in the X direction with a tendency to *local equilibrium*, we call the

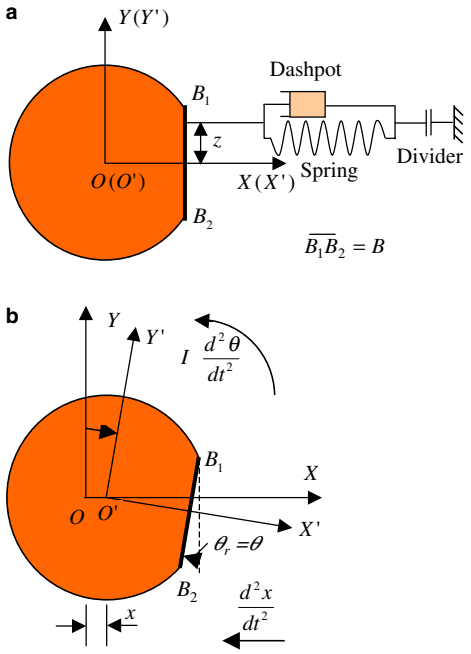

Fig. 8. Motions of a grain with rolling resistence at contact: (a) initial position; (b) current position.

local equilibrium condition. In Fig. 8(b), $O'X'Y$ does not coincide with OXY. Denote by x the displacement of the grain centre along X axis, and by θ the rotation of the grain about the centre of mass respectively. Denote by m and I the mass of the grain and the mass momentum of inertia of the grain about the centre of mass respectively. In addition, let η_n be the damping parameter for the Newtonian dashpot of the normal BE, according to Eq. (25c). Note that the total relative rotation θ_r of B_1B_2 about its initial position is equal to θ in Fig. 8.

The damping force f_η (in N/m) of the Newtonian dashpot, which is taken as positive in positive X axis, is velocity-dependent and calculated by

$$f_\eta = \eta_n(\dot{\theta}_r z - \dot{x}). \tag{37}$$

The total force f_n by the normal BE, resulting from both the spring and the dashpot at this instant, reads

$$f_n = k_n(-x + \theta_r z) + \eta_n(\dot{\theta}_r z - \dot{x}). \tag{38}$$

Eq. (38) leads to the resultant force F_n (in N) due to the continuously distributed normal BE as follows:

$$F_n = \int_{-B/2}^{B/2} [k_n(-x + \theta_r z) + \eta_n(\dot{\theta}_r z - \dot{x})]\, \mathrm{d}z. \tag{39}$$

Based on Newton's second law, the acceleration $\ddot{x}$ of the mass will then be obtained

$$m\ddot{x} = \int_{-B/2}^{B/2} [k_n(-x + \theta_r z) + \eta_n(\dot{\theta}_r z - \dot{x})]\, \mathrm{d}z. \tag{40}$$

Eq. (40) can be rewritten as follows

$$m\ddot{x} + a_1\dot{x} + a_2\dot{\theta}_r + a_3 x + a_4\theta_r = 0, \tag{41}$$

where a_1, a_2, a_3 and a_4 are constants defined by

$$a_1 = \eta_n B, \quad a_2 = a_4 = 0, \quad a_3 = k_n B. \tag{42a, b, c}$$

Similarly, for angular motion, the moment M' due to the normal BE about the mass centre at this instant, in which counter-clockwise rotation is positive, is

$$M' = -k_n(-x + \theta_r z)z - \eta_n(\dot{\theta}_r z - \dot{x})z. \tag{43}$$

Eq. (43) leads to the resultant couple M by the continuously distributed normal BE

$$M = -\int_{-B/2}^{B/2} [k_n(-x + \theta_r z) + \eta_n(\dot{\theta}_r z - \dot{x})] \cdot z \, dz. \tag{44}$$

Hence, the equation for angular motion can be expressed as

$$I\ddot{\theta} + \int_{-B/2}^{B/2} [k_n(-x + \theta_r z) + \eta_n(\dot{\theta}_r z - \dot{x})] \cdot z \, dz = 0. \tag{45}$$

Rewriting Eq. (45) leads to

$$I\ddot{\theta} + a_5\dot{\theta}_r + a_6\theta_r + a_2\dot{x} + a_4 x = 0, \tag{46}$$

where a_2 and a_4 are defined in Eq. (42b). a_5 and a_6 are defined, respectively, by

$$a_5 = \eta_n \frac{B^3}{12}, \quad a_6 = k_n \frac{B^3}{12}. \tag{47a, b}$$

Using Eq. 42b, Eqs. (41) and (46) become

$$m\ddot{x} + a_1\dot{x} + a_3 x = 0, \quad I\ddot{\theta} + a_5\dot{\theta}_r + a_6\theta_r = 0. \tag{48a, b}$$

Eq. (48a) is the equation governing the translational motion of the grain for this reduced problem, and can be found in any engineering mechanics textbook on kinematics of rigid body. It confirms our previous statement that rolling resistance (couple) does not affect the translational motions of grains. Eq. (48b) is the governing equation to include the effect of rolling resistance on the angular motion of the grain for this reduced problem. These two equations will lead to *local equilibrium* solutions, and hence they satisfy the *local equilibrium condition*.

From Eqs. (25), (29), (42) and (47), we obtain

$$a_1 = \mu_n, \quad a_3 = K_n, \quad a_5 = \mu_n \frac{(r \cdot \delta)^2}{12} = \mu_m,$$
$$a_6 = K_n \frac{(r \cdot \delta)^2}{12} = K_m, \tag{49a, b, c, d}$$

where μ_m is here termed as the *rolling damping parameter*, which is determined by normal damping parameter μ_n, common radius r and the shape parameter δ in Eq. (49c). Hence, Eqs. (48) can be re-written in terms of the model parameters by

$$m\ddot{x} + \mu_n\dot{x} + K_n x = 0, \quad I\ddot{\theta} + \mu_m\dot{\theta}_r + K_m\theta_r = 0, \tag{50a, b}$$

μ_m and K_m in Eqs. (50) are directly linked to μ_n and K_n, respectively, through δ. Hence, again, only δ needs to be introduced in the governing equations when compared with the standard DEMs [14,15]. In addition, Eqs. (50) satisfy the requirement of local equilibrium.

The governing equations given above are for a grain with single contact with a wall, in which contact is continuously distributed with normal BE, with its displacement assumed to be along the X direction only. Indeed, Eqs. (50) can be rewritten as follows:

$$m\ddot{x} = -(\mu_n\dot{x} + K_n x) = F_n = F_x, \quad I\ddot{\theta} = -(\mu_m\dot{\theta}_r + K_m\theta_r) = M. \tag{51a, b}$$

Note that the right-hand sides of Eqs. (51) are the component of force F_x in the X direction and the couple, respectively, acting at a single contact in this reduced problem, which are dependent on the contact properties. The left-hand sides of Eqs. (51) represent the grain's instantaneous accelerations.

4.2. Grain with several contacts in a general case

We now turn to a general case that a grain has several contacts, with walls or other grains, in a general case a grain contact is continuously distributed with normal/tangential BE. It is known that rolling resistance (couple) does not affect the translational motions of grains but does affect the angular motion of grains. Hence, the couple at each direct contact must be summed up in affecting the angular motion of a grain. For disc j with radius r_j, the contact forces $F_n^{(q)}$, $F_s^{(q)}$ and couple $M^{(q)}$ are summed over p neighbours, which then govern the motion of the disc in both X and Y directions and the rotation about the center of mass

$$\ddot{x}_i^j = \frac{1}{m^j}\sum_{q=1}^{p} F_i^{(q)}, \quad \ddot{\theta}^j = \frac{1}{I^j}\left(\sum_{q=1}^{p} r_j F_s^{(q)} + \sum_{q=1}^{p} M^{(q)}\right), \tag{52a, b}$$

where $F_i^{(q)}$ is x_i component of the resultant force at contact q and $i = 1, 2$, representing X and Y directions, respectively.

Eqs. (52) are similar to those used by Iwashita and Oda [48,49]. However, Eqs. (52) naturally satisfy the requirement of local equilibrium since they are derived from Eqs. (50), while local equilibrium has not been discussed in [48,49]. The governing equations when compared with standard DEMs [14,15] are revised by the same parameter δ. In comparison, μ_m and K_m as used in [48,49] are two additional parameters chosen independently by trial and error in their DEM analyses. It is not difficult to see, in some cases, the choices of the two rolling parameters may not satisfy the requirement of local equilibrium.

When $\delta = 0$, we obtain $B = 0$ and Eqs. (52) reduce to those used in a standard DEM as

$$\ddot{x}_i^j = \frac{1}{m^j}\sum_{q=1}^{p} F_i^{(q)}, \quad \ddot{\theta}^j = \frac{1}{I^j}\sum_{q=1}^{p} r_j F_s^{(q)}. \tag{53a, b}$$

In summary, Table 1 provides main comparison between the model in [48,49] and that in this study. Table 1 shows that our model differs from [48,49] on several aspects:

- In kinematic model, we propose complete and general definitions of pure sliding and pure rolling while they did not; the displacements of contact are described with rolling and sliding components in a complete and general formulation with theoretical proof here while their work was given for a pair of same-sized particles without proof; they gave an empirical relation between contact displacement and relative rotation without proof, while we present a theoretical relationship with proof; the displacements of contact are related to energy dissipation here, which was not discussed in [48,49].
- In contact model, our model is established on a physical model that a contact width B is a continuously distributed system of normal and tangential basic elements, which was absent in their study; B depends on grain size, controlled by new model parameter δ in our model, while their is a variable depending on normal force, normal stiffness value and grain size etc.; our rolling resistance model can provide elasto-plastic or elasto-brittle-plastic performance, hence includes theirs; no new parameter is needed in our theoretically derived rolling resistance model, while three empirical parameters are introduced in theirs, i.e., rolling stiffness, peak rolling resistance and rolling damping.
- In governing equations, our equation governing rotational motion of grain satisfies the requirement of local equilibrium, while theirs may not.

Hence, the mathematical model proposed here can be regarded as an improvement/refinement of the models used in [48,49].

5. Further discussion

5.1. DEM code and simulation conditions

The model presented here has been implemented into a two-dimensional DEM code by the authors, which was originally developed by one of the authors for special soils [58,59], with techniques similar to that proposed by Cundall and Strack [14,15]. Fifty-four numerical simulations have been carried out with the revised 2D DEM code to study the frictional behaviour of the granular materials incorporating the proposed model.

Granular materials with a distribution of grain size shown in Fig. 9 have been used in our DEM analyses. The materials modelled are all composed of discs with a maximum diameter of 9.0 mm, and a minimum diameter of 6.0 mm, an average grain diameter $d_{50} = 7.6$ mm and uniformity coefficient $C_u = d_{60}/d_{10} = 1.3$. The multi-layer undercompaction technique proposed by one of the authors [58] was used to prepare a type of medium-dense specimen with planar void ratio 0.25. The reader is referred to this reference for further details. Note that the *shape parameter* δ was set to zero in the sample preparation so that all samples have the same initial void ratio and fabric before choosing different values of δ. After the samples were generated, δ was set to zero to model a no rolling resistance material, and 0.1–1.6 for a rolling resistance material, respectively. For the latter material, elasto-plastic (Model 1) and elasto-brittle-plastic (Model 2) rolling contact models were chosen, respectively. Fig. 10 presents a typical specimen before testing. Each specimen has a width of 180 mm and a height of 306.7 mm, and is composed of 1008 grains. The small number of discs was chosen in consideration of the present capacity of desktop computers in order to make the study feasible.

Biaxial compression tests were carried out on each sample, with consolidation under a given isotropic stress followed by constant vertical compressive strain rate as 0.2%/min under constant horizontal stress value σ_h. The vertical strain rate is defined as the ratio of change of specimen height to its current height during each incremental time. During the tests, vertical stress value σ_v on boundary was continuously observed. The consolidation stresses were taken to be 100, 200, 400 kPa, respectively. A total of 54 numerical tests have been performed on different kinds of materials, with three tests on no rolling resistance, Model 1 materials of $\delta = 0.1$–1.6 and Model 2 material of $\delta = 0.4$, respectively. The large value of δ corresponds to angular shape grains in essence by means of discs. The normal and the tangential spring stiffness were chosen as 2.0×10^8 and 1.5×10^8 (N/m), respectively, with a coefficient of interparticle friction 0.5. Friction as well as rolling resistance is set to zero at wall–particle contacts in all tests in order to diminish the effect of boundaries. Discussions will be mainly on frictional behaviour of granular materials.

5.2. Frictional behaviour of granular materials of different models

Fig. 11 presents the stress–strain behaviour obtained from the medium-dense materials for no rolling resistance, Model 1 and Model 2 of $\delta = 0.4$, under confining stress 200 kPa. The deviatoric stress and volumetric strain, in Figs. 11(a) and (b), respectively, are defined

Table 1
Main comparison between the model in [48,49] and that in this study

	Iwashita and Oda [48,49]		This study	
	Formula	Main features	Formula	Main features
Kinematic model				
Definition of pure rolling displacement	Not given	N/A	$\begin{cases} \mathrm{d}a = -\mathrm{d}b \neq 0 \\ \mathrm{d}U_\mathrm{s} = 0, \quad \mathrm{d}U_\mathrm{r} = \mathrm{d}a \end{cases}$	Complete and general definition
Definition of pure sliding displacement	Not given	N/A	$\begin{cases} \mathrm{d}a = \frac{r_1}{r_2}\mathrm{d}b, \quad \mathrm{d}a \neq 0 \text{ or } \mathrm{d}b \neq 0 \\ \mathrm{d}U_\mathrm{s} = \frac{\mathrm{d}a+\mathrm{d}b}{2}, \quad \mathrm{d}U_\mathrm{r} = 0 \end{cases}$	Complete and general definition
Decomposition of contact displacements	$\mathrm{d}a = \mathrm{d}U_\mathrm{r} + \mathrm{d}U_\mathrm{s}$ $\mathrm{d}b = -\mathrm{d}U_\mathrm{r} + \mathrm{d}U_\mathrm{s}$	For $r_1 = r_2$ without proof	$\mathrm{d}a = \mathrm{d}U_\mathrm{r} + \frac{2r_1}{r_1+r_2}\mathrm{d}U_\mathrm{s}$ $\mathrm{d}b = -\mathrm{d}U_\mathrm{r} + \frac{2r_2}{r_1+r_2}\mathrm{d}U_\mathrm{s}$	Complete and general decomposition with theoretical proof
Relation between contact displacement and relative rotation	$\mathrm{d}\theta_\mathrm{r} = \frac{\mathrm{d}U_\mathrm{r}}{r'}$ $r' = (r_1 + r_2)/2$	Empirical relation without proof	$\mathrm{d}\theta_\mathrm{r} = 2\dfrac{\mathrm{d}U_\mathrm{r}}{r}, \quad r = \dfrac{2r_1r_2}{r_1+r_2}$	Theoretical relationship with proof
Related to energy dissipation	Not given	N/A	Yes	Theoretical proof
Contact model				
Physical model	Not given	N/A	A contact width is a continuously distributed system of normal and tangential basic elements	A reasonable and theoretical assumption
Contact with B	Depending on normal force, normal stiffness value and grain size, etc.	A variable	$B = \delta \cdot r, \quad r = \dfrac{2r_1r_2}{r_1+r_2}$	Depending on grain size, controlled by new model parameter δ
Response of rolling model	Elasto-plastic	One model	Elasto-plastic or elasto-brittle-plastic	Two models, including [48]
Rolling stiffness	Chosen by trial and error or $K_m = K_\mathrm{s}\, r'^2$	Empirical, parameter K_m needed	$K_m = \frac{K_n \cdot r^2}{12}\delta^2$	Theoretical solution without introduction of new parameter
Peak rolling resistance	$M_0 = \eta F_n$ or $M_0 = M_\mathrm{max}$	Empirical, parameter η or M_max needed	$M_0 = \frac{1}{6}F_n r\delta$	Theoretical solution without introduction of new parameter
Rolling damping	C_r, chosen by trial and error	Empirical, parameter C_r needed	$\mu_m = \mu_n \frac{(r\cdot\delta)^2}{12}$	Theoretical solution without introduction of new parameter
Number of parameters in rolling model	Three parameters and one variable	More	One parameter	Fewer
Governing equations				
Rotational motion of grain	Similar to this study	Local equilibrium neglected	$\ddot{\theta}^j = \frac{1}{J^j}\left(\sum_{q=1}^{\mathrm{p}} r_j F_\mathrm{s}^{(q)} + \sum_{q=1}^{\mathrm{p}} M^{(q)}\right)$	Satisfying local equilibrium

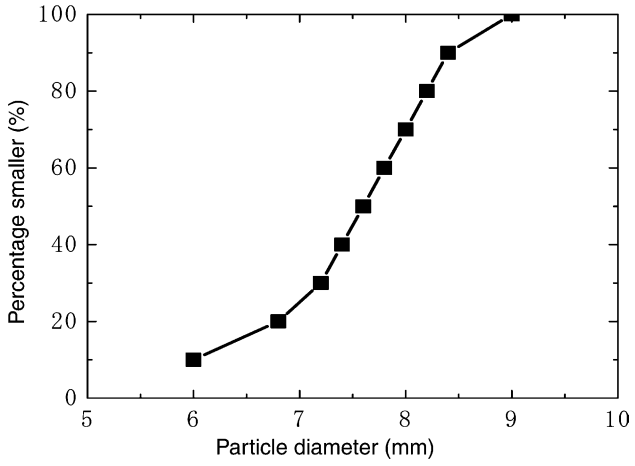

Fig. 9. Distribution of grain size used in the DEM analyses.

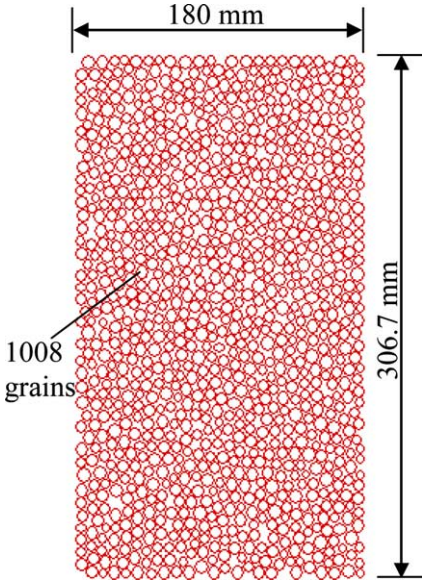

Fig. 10. A typical assembly of grains used in the DEM analyses.

as $(\sigma_v - \sigma_h)/2$ and $(\varepsilon_v + \varepsilon_h)$. Fig. 11 shows that all these three models predict a strain-softening and shear-dilantant behaviour, which reflects one main feature of the medium-dense granular material. However, Fig. 11 also shows these models can lead to some differences in the stress–strain behaviour, even though under the same confining stress. It can be seen from Fig. 11(a) that Model 1 (elasto-plastic rolling model) predicts the largest three values: initial stiffness, peak strength and difference between the peak and residual strength; while the no rolling resistance model gives rise to the smallest. In addition, Fig. 11(b) demonstrates that Model 1 gives a prediction of the largest initial compression and the subsequent dilantancy, while the no rolling resistance model produces the smallest. These observations are in agreement with those in [48,49]. In contrast, Model 2 (elasto-brittle-plastic rolling model) seems to give prediction of these values in between.

Fig. 12 provides the peak/residual strength envelopes of the medium-dense materials for no rolling resistance, Model 1 and Model 2 of $\delta = 0.4$, obtained from nine DEM biaxial compression tests of different σ_h. The strength envelopes are expressed in terms of mean stress $(\sigma_h + \sigma_v)/2$ and deviatoric stress $(\sigma_v - \sigma_h)/2$. In the figure, ϕ^p (ϕ^r), ϕ_1^p (ϕ_1^r) and ϕ_2^p (ϕ_2^r) are peak (residual) friction angle obtained from the materials of no rolling resistance, Model 1 and Model 2, respectively, which method will be introduced later. Fig. 12 shows that all strength envelopes of no rolling resistance materials nearly pass through the origin, confirming that the material is cohesionless. The small amount of 'apparent cohesion' is found for the materials of rolling resistance, which indicates that rolling resistance may act as a kind of 'interlocking' and hence can lead to additional shear strength. This is in agreement with the subsequent observation in Fig. 12 that the predicted peak (residual) internal friction angle ϕ deduced from the envelopes by $\sin\phi = (\sigma_v - \sigma_h)/(\sigma_v + \sigma_h)$ is equal to 24.4°, 26.5° and 29.0° (19.3°, 20.7° and 23.0°) for no rolling resistance, Model 2 and Model 1 material, respectively. In addition,

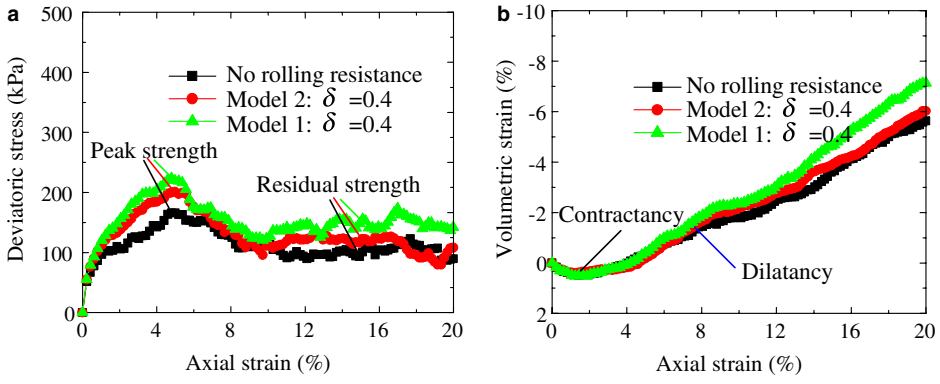

Fig. 11. Stress–strain behaviour obtained from the materials of no rolling resistance, Model 1 and Model 2 of $\delta = 0.4$, respectively, under confining stress 200 kPa: deviatoric stress $(\sigma_v - \sigma_h)/2$ against axial strain (a); volumetric strain against axial strain (b).

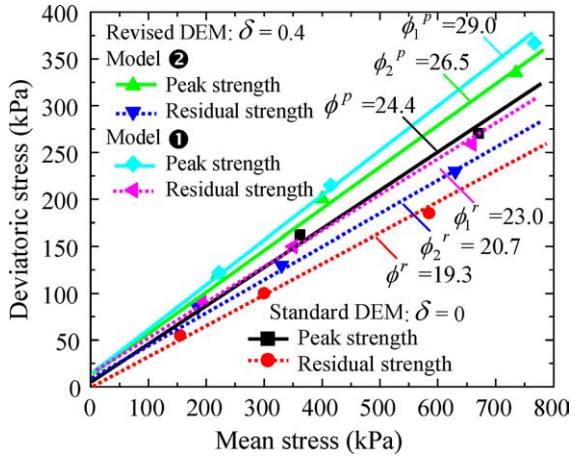

Fig. 12. Strength envelopes of the material for different rolling contact models, deduced from nine DEM biaxial compression tests.

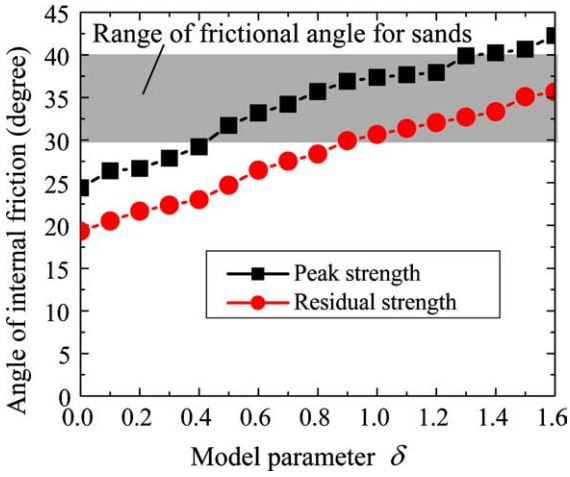

Fig. 13. Relationship between the angle of internal friction and model parameter δ for rolling resistance Model 1, deduced from 51 DEM biaxial compression tests.

the peak/residual ϕ of the material with elasto-brittle-plastic (Model 2) rolling contact model, i.e., 26.5°/20.7°, is smaller than that of Model 1 (28.8°/22.8°), which is consistent with known facts on crushable materials [57]. Furthermore, the predicted residual ϕ of the material with no rolling resistance (19.3°) is much smaller in comparison with its coefficient of interparticle friction of 0.5 which leads to $\phi = \arctan(0.5) = 26.5°$, which is also in an agreement with the previous works by other researchers [32–35]. For example, Thornton [35] indicates that such a small value is normal with models that ignore the possibility of particle rolling resistance at contacts. However, the analyses show that ϕ of granular materials can be increased with the use of the proposed models.

5.3. Frictional behaviour of granular materials of Model 1

We shall now further discuss the effect of different values of parameter δ on the angle of internal friction ϕ by considering granular materials of the rolling resistance Model 1.

Fig. 13 presents relationships between peak (residual) ϕ and δ for rolling resistance Model 1, deduced from the 51 DEM biaxial compression tests. Fig. 13 shows that the peak (residual) ϕ increases evidently with the increasing of δ. When δ is increased from 0.0 to 1.6, the peak (residual) ϕ changes from 24.4° (19.3°) to 42.3° (35.8°). Note that internal friction angle of real granular materials is usually between 30° and 40°. A number of researchers have implemented elliptical or other shaped particles to inhibit particle rolling in order to increase, and hence produce more realistic, strength values [33,36–39]. Efficient methods of increasing the strength include inducing clustering of the discs [38] and using angular grains [39]. In most studies, the increase of strength appears to be due to the fabric of the non-spherical assembly. For example, it is reported that randomly oriented ellipses showed less than a 5° increase in strength over discs [36]. In addition, it can be also found that using Hertz's contact theory to determine the normal contact stiffness, can only produce a residual internal friction angle of about 23° [60]. It then can be found that, in our case, even for circular discs, the predicted ϕ here can be increased to a realistic value in the materials due to the presence of the rolling resistance, provided that the value of δ is properly chosen. Furthermore, the models are very easily implemented in standard DEMs [14,15]. Note that the increase of ϕ with the increasing of δ does not lead to 'the increase of ϕ against particle sizes', i.e., size-dependence. This is because, as shown by Eq. (24), given a particle size (contact width), δ is proportional (inverse) to contact width (particle sizes). In addition, the difference between peak and residual strength is almost constant with δ. This may be due to the fact that the rolling resistance Model 1, the elastic–plastic model, was used in the numerical simulations. Hence, the rolling resistance, which is controlled by δ, may give the same contribution to both peak and residual strength.

6. Concluding remarks

This paper presented a novel discrete model for granular materials with rolling resistance, which can be easily implemented in DEMs. Compared to other works [48,49], the main advantages of our model are: (a) it is derived on graphical and mechanical bases and satisfies the requirement of local equilibrium; (b) it requires one additional parameter δ in comparison to the standard DEMs [14,15]. The model proposed is an improvement to that used by Iwashita and Oda [48,49]. The main conclusions are as follows:

(1) Based on the new definitions of pure sliding and pure rolling, the displacement of contact can be rigorously decomposed into rolling and sliding components in a unique way, which is different from and is more proper than [48,49]. Our theoretical proof shows that both components play an important role in energy dissipation for granular materials with rolling resistance.
(2) Using the proposed micro-mechanical model that a particle contact width is continuously distributed with normal/tangential basic element, a rolling contact model is rigorously established together with normal and tangential contact models. This rolling contact model can be simplified as elasto-plastic or elasto-brittle-plastic model with physical interpretation, thus includes that in [48,49]. The equations governing the motion of particles satisfy the requirement of local equilibrium, an issue not discussed in [48,49]. Only one parameter δ is needed in comparison to the standard DEMs [14,15], and apparently fewer than those in [48,49] (three chosen separately by trial and error, and fourth related to particle overlap in value [48,49]).
(3) The 54 numerical simulations carried out by the modified DEM developed by the authors show that, the coefficient of internal friction ϕ of granular materials can be increased to a reasonable value with the use of the proposed model, by properly choosing the value of δ in the δ–ϕ relationship established in this paper. Such increase of ϕ is very difficult to obtain by other methods in the literature, such as ellipse-shaped particles.
(4) The models are applicable to elliptical or other shaped particles. The models can provide assistance in microanalysis such as strain localization analysis and developing elastic micro-mechanical models of granular media, such as micro-mechanical models incorporating both contact anisotropy and rolling resistance [61], considering that there are still open questions on such topics as the asymmetry of stress tensor of granular material [20,25,55]. They can also be helpful to other important works, such as the theoretical framework for the statics and kinematics of discrete Cosserat-type granular materials [62], mechanical behaviour and failure of cohesive granular materials [63] and fracture analysis [64]. In addition, the models presented can be extended for three-dimensional system, which is one of our future tasks.

Acknowledgements

The work reported here was funded by an EPSRC grant with number GR/R85792/01. The authors thank the EPSRC for the financial support of the first author during his post-doctoral research on this study.

Appendix A. Decomposition of contact displacements

The contact displacements $\mathrm{d}a$ and $\mathrm{d}b$ are both composed of rolling and sliding components, denoted by $\mathrm{d}U_\mathrm{r}$ and $\mathrm{d}U_\mathrm{s}$, respectively. $\mathrm{d}a$ and $\mathrm{d}b$ is postulated to be uniquely expressed in the following linear functions of $\mathrm{d}U_\mathrm{r}$ and $\mathrm{d}U_\mathrm{s}$, respectively

$$\mathrm{d}a = a_1\mathrm{d}U_\mathrm{r} + a_2\mathrm{d}U_\mathrm{s}, \quad \mathrm{d}b = b_1\mathrm{d}U_\mathrm{r} + b_2\mathrm{d}U_\mathrm{s}, \quad \text{(A.1a, b)}$$

where a_1, a_2, b_1, b_2 are constants to be determined below.

From Eqs. (A.1), $\mathrm{d}U_\mathrm{r}$ and $\mathrm{d}U_\mathrm{s}$ can be retrieved in terms of $\mathrm{d}a$ and $\mathrm{d}b$, respectively, as follows:

$$\mathrm{d}U_\mathrm{r} = \frac{b_2\mathrm{d}a - a_2\mathrm{d}b}{a_1b_2 - a_2b_1}, \quad \mathrm{d}U_\mathrm{s} = \frac{b_1\mathrm{d}a - a_1\mathrm{d}b}{a_2b_1 - a_1b_2}. \quad \text{(A.2a, b)}$$

Based on the new definitions of pure rolling and pure sliding described for two discs 1 and 2 with radii r_1 and r_2

$$\begin{cases} \mathrm{d}a = -\mathrm{d}b \neq 0 \\ \mathrm{d}U_\mathrm{s} = 0, \quad \mathrm{d}U_\mathrm{r} = \mathrm{d}a \end{cases} \text{for pure rolling} \quad \text{(A.3a, b)}$$

$$\begin{cases} \mathrm{d}a = \frac{r_1}{r_2}\mathrm{d}b, \quad \mathrm{d}a \neq 0 \text{ or } \mathrm{d}b \neq 0 \\ \mathrm{d}U_\mathrm{s} = \frac{\mathrm{d}a+\mathrm{d}b}{2}, \quad \mathrm{d}U_\mathrm{r} = 0 \end{cases} \text{for pure sliding} \quad \text{(A.4a, b)}$$

the solution to a_1, a_2, b_1, b_2 in Eqs. (A.1) can be obtained uniquely as

$$a_1 = 1, \quad b_1 = -1, \quad a_2 = \frac{2r_1}{r_1 + r_2}, \quad b_2 = \frac{2r_2}{r_1 + r_2}. \quad \text{(A.5a, b, c, d)}$$

Hence, $\mathrm{d}a$ and $\mathrm{d}b$ in Eqs. (A.1) can be expressed explicitly in a linear function of $\mathrm{d}U_\mathrm{r}$ and $\mathrm{d}U_\mathrm{s}$, respectively, as follows:

$$\mathrm{d}a = \mathrm{d}U_\mathrm{r} + \frac{2r_1}{r_1 + r_2}\mathrm{d}U_\mathrm{s}, \quad \mathrm{d}b = -\mathrm{d}U_\mathrm{r} + \frac{2r_2}{r_1 + r_2}\mathrm{d}U_\mathrm{s} \quad \text{(A.6a, b)}$$

with inverse relations

$$\mathrm{d}U_\mathrm{r} = \frac{r_2\mathrm{d}a - r_1\mathrm{d}b}{r_1 + r_2}, \quad \mathrm{d}U_\mathrm{s} = \frac{\mathrm{d}a + \mathrm{d}b}{2}. \quad \text{(A.7a, b)}$$

Appendix B. Expression of incremental work at contact

We shall consider incremental work at particle contact k. The total incremental work of an assembly can be obtained by accumulating the incremental work of

each contact over all contacts the whole assembly. During a time interval from t to $t + \mathrm{d}t$, the tangential contact force and the couple at contact k are assumed to change linearly from F_s^k and M^k to $(F_s^k + \mathrm{d}F_s^k)$ and $(M^k + \mathrm{d}M^k)$, respectively. In the time interval $\mathrm{d}t$, it has been proven in Appendix A that contact displacements $\mathrm{d}a$ and $\mathrm{d}b$ can be expressed explicitly as a linear function of rolling and sliding components, $\mathrm{d}U_r$ and $\mathrm{d}U_s$, respectively. Hence, the incremental work $\mathrm{d}W^k$ done at the contact by the tangential force and the couple to two discs 1 and 2 with radii r_1 and r_2 are

$$\mathrm{d}W^k = \frac{\left(2F_s^k + \mathrm{d}F_s^k\right)\mathrm{d}a}{2} + \frac{\left(2F_s^k + \mathrm{d}F_s^k\right)\mathrm{d}b}{2m_1} + \frac{\left(2M^k + \mathrm{d}M^k\right)\mathrm{d}a}{2r_1} + \frac{\left(2M^k + \mathrm{d}M^k\right)\mathrm{d}b}{2r_2m_2}, \tag{B.1}$$

where m_1, m_2 may be +1 or −1 and the signs need to be determined below.

The expression, Eq. (B.1), for the incremental work must be able to describe two special cases. Let us first consider a special case that the contact k is shared by two discs which undergo pure sliding defined by

$$\begin{cases} \mathrm{d}a = \frac{r_1}{r_2}\mathrm{d}b, \quad \mathrm{d}a \neq 0 \text{ or } \mathrm{d}b \neq 0, \\ \mathrm{d}U_s = \frac{\mathrm{d}a+\mathrm{d}b}{2}, \quad \mathrm{d}U_r = 0. \end{cases} \tag{B.2a, b}$$

Assuming that the discs are of equal radius, and $M^k = 0$, $\mathrm{d}M^k = 0$, i.e., no couple exists at the contact, then $\mathrm{d}W^k$ in Eq. (B.1) can be expressed as

$$\mathrm{d}W^k = \frac{\left(2F_s^k + \mathrm{d}F_s^k\right)}{2}\left(\mathrm{d}a + \frac{\mathrm{d}b}{m_1}\right). \tag{B.3}$$

Since $\mathrm{d}a = \mathrm{d}b$ is obtained from Eq. (B.2a) in this case, the choice of $m_1 = -1$ would lead to $\mathrm{d}W^k$ being always zero, hence, we must take $m_1 = 1$ in Eq. (B.3).

Next consider the case that the contact k shared by two particles undergoes a pure rolling defined by

$$\begin{cases} \mathrm{d}a = -\mathrm{d}b \neq 0, \\ \mathrm{d}U_s = 0, \quad \mathrm{d}U_r = \mathrm{d}a. \end{cases} \tag{B.4}$$

Considering that $M^k \neq 0$, $\mathrm{d}M^k \neq 0$, $\mathrm{d}a = -\mathrm{d}b$ in this case, given $m_1 = 1$, then $\mathrm{d}W^k$ in Eq. (B.1) can be expressed as

$$\mathrm{d}W^k = \frac{\left(2M^k + \mathrm{d}M^k\right)}{2}\left(\frac{\mathrm{d}a}{r_1} + \frac{\mathrm{d}b}{m_2r_2}\right) = \frac{\left(2M^k + \mathrm{d}M^k\right)}{2r}\mathrm{d}a(1 - m_2) \tag{B.5}$$

for discs of equal radius. Then $m_2 = 1$ would lead to a zero value of $\mathrm{d}W^k$ in pure rolling, to satisfy the requirement that $\mathrm{d}W^k$ be non-zero in pure rolling, we must have $m_2 = -1$ in Eq. (B.5).

Returning now to the general case, by substituting $m_1 = 1$ and $m_2 = -1$ into Eq. (B.1), a general formula for $\mathrm{d}W^k$ results

$$\mathrm{d}W^k = \frac{\left(2F_s^k + \mathrm{d}F_s^k\right)(\mathrm{d}a + \mathrm{d}b)}{2} + \left(2M^k + \mathrm{d}M^k\right)\left(\frac{\mathrm{d}a}{2r_1} - \frac{\mathrm{d}b}{2r_2}\right). \tag{B.6}$$

References

[1] Yu H-S. CASM: A unified state parameter model for clay and sand. Int J Numer Anal Meth Geomech 1998;22:621–53.

[2] Wang ZL, Dafalias YF, Shen CK. Bounding surface hypoplasticity model for sand. ASCE J Eng Mech 1990;116:983–1001.

[3] Kolymbas D. An outline of hypoplasticity. Arch Appl Mech 1991;61:143–51.

[4] Iai S, Matsunaga Y, Kameoka T. Strain space plasticity model for cyclic mobility. Soils Foundations 1992;32:1–15.

[5] Li XS, Dafalias YF. A constitutive framework for anisotropic sand including non-proportional loading. Géotechnique 2004;54(1):41–55.

[6] Spencer AJM. A theory of the kinematics of ideal soils under planer strain conditions. J Mech Phys Solids 1964;12:337–51.

[7] De Josselin de Jong G. The double sliding, free rotating model for granular assemblies. Géotechnique 1971;21:155–62.

[8] Harris D. A unified formulation for plasticity models of granular and other materials. Proceedings of the Royal Society London A 1995;450:37–49.

[9] Spencer AJM. Double-shearing theory applied to instability and strain localization in granular materials. J Eng Math 2003;45:55–74.

[10] Mühlhaus HB, Vardoulakis I. The thickness of shear bands in granular materials. Géotechnique 1987;37:271–83.

[11] Vardoulakis I. Shear-banding and liquefaction in granular materials on the basis of a Cosserat continuum theory. Ingenieur Archive, Berlin, Germany 1989;59(2):106–14.

[12] Vardoulakis I, Aifantis EC. Gradient dependent dilatancy and its implications in shear banding and liquefaction. Ingenieur Archive, Berlin, Germany 1989;59:197–208.

[13] Zbib HM, Aifantis EC. A gradient-dependent flow theory of plasticity: application to metal and soil instabilities. Appl Mech Rev 1989;42:295–304.

[14] Cundall PA, Strack ODL. The distinct element method as a tool for research in granular media. Part II. Department of Civil Engineering Report, University of Minnesota, Minnesota; 1979.

[15] Cundall PA, Strack ODL. The distinct numerical model for granular assemblies. Géotechnique 1979;29:47–65.

[16] Bardet JP, Proubet J. A numerical investigation of the structure of persistent shear bands in granular media. Géotechnique 1991;41:599–613.

[17] Oda M, Konishi J, Nemat-Nasser S. Experimental micromechanical evaluation of strength of granular materials: effects of particle rolling. Mech Mater 1982;1:269–83.

[18] Oda M, Kazama H. Micro-structure of shear band and its relation to the mechanism of dilatancy and failure of granular soils. Géotechnique 1998;48:465–81.

[19] Chang CS, Liao CL. Constitutive relation for a particulate medium with effect of particle rotation. Int J Solids Struct 1990;26:437–53.

[20] Chang CS, Ma L. A micromechanically-based micropolar theory for deformation of granular solids. Int J Solids Struct 1991;28:67–86.

[21] Chang CS, Gao J. Second-gradient constitutive theory for granular material with random packing structure. Int J Solids Struct 1995;32:2279–93.

[22] Harris WW, Viggiani G, Mooney MA, Finno RJ. Use of stereophoto-grammetry to analyze the development of shear bands in sand. ASTM Geotech Testing J 1995;18:405–20.
[23] White DJ, Take WA, Bolton MD. Soil deformation measurement using particle image velocimetry (PIV) and photogrammetry. Géotechnique 2003;53(7):619–31.
[24] Tordesillas A, Walsh DCS. Incorporating rolling resistance and contact anisotropy in micromechanical models of granular media. Powder Technol 2002;124:106–11.
[25] Ehlers W, Ramm E, Diebels S, D'Addetta GA. From particle ensembles to Cosserat continua: homogenization of contact forces towards stresses and couple stresses. Int J Solids Struct 2003;40:6681–702.
[26] Bagi K. On the definition of stress and strain in granular assemblies through the relation between micro- and macro-level characteristics. In: Thornton C, editor. Powders & grains 93. Rotterdam: Balkema; 1993. p. 117–21.
[27] Bardet JP. Observations on the effects of particle rotations on the failure of idealized granular materials. Mech Mater 1994;18:159–82.
[28] Calvetti F, Combe G, Lanier J. Experimental micromechanical analysis of a 2D granular material: relation between structure evolution and loading path. Mech Cohesive Fric Mater 1997;2:121–63.
[29] Misra A, Jiang H. Measured kinematic fields in the biaxial shear of granular materials. Comput Geotech 1997;20:267–85.
[30] Dedecker F, Chaze M, Dubujet P, Cambou B. Specific features of strain in granular materials. Mech Cohesive Fric Mater 2000;5:173–9.
[31] Kuhn MR, Bagi K. Particle rotations in granular materials. In: Smyth AW, editor. 15th ASCE engineering mechanics conference, June 2–5, Columbia University, New York; 2002. Available from: http://www.civil.columbia.edu/em2002/.
[32] Ting JM, Corkum BT, Kauffman CR, Greco C. Discrete numerical model for soil mechanics. ASCE J Geotech Eng 1989;115:379–98.
[33] Rothenburg L, Bathurst RJ. Micromechanical features of granular assemblies with planar elliptical particles. Géotechnique 1992;42:79–95.
[34] Ng TT, Dobry R. A nonlinear numerical model for soil mechanics. ASCE J Geotech Eng 1994;120:388–403.
[35] Thornton C. Numerical simulation of deviatoric shear deformation of granular media. Géotechnique 2000;50:43–53.
[36] Oda M. A micro-deformation model for dilatancy of granular materials. In: Chang CS et al., editors. Symposium on mechanics of particulate materials in McNu conference. ASCE; 1997. p. 24–37.
[37] Ting JM, Meechum LR, Rowell JD. Effect of particle shape on the strength and deformation mechanism of ellipse-shaped granular assemblages. Eng Comput 1995;12:99–108.
[38] Sawada S, Pradhan TBS. Analysis of anisotropy and particle shape by distinct element method. In: Siriwardane, Zaman, editors. Computer methods and advancements in geomechanics. Rotterdam, The Nethelands: Balkema; 1994. p. 665–70.
[39] Thomas PA, Bray JD. Capturing nonspherical shape of granular media with disk clusters. ASCE J Geotech Geoenviron Eng 1999;125:169–78.
[40] Ullidtz P. Modelling of granular materials using the discrete element method. Proceedings of 8th international conference on asphalt pavements, August 10–14, Seattle, Washington, vol. 1. Seattle, WA, USA: University of Washington; 1997. p. 757–69.
[41] Mustoe GGW, Miyata M. Material flow analyses of noncircular-shaped granular media using discrete element methods. ASCE J Eng Mech 2002;127:1017–26.
[42] Ng TT. Fabric evolution of ellipsoidal arrays with different particle shapes. ASCE J Eng Mech 2002;127:994–9.
[43] Mirghasemi AA, Rothenburg L, Matyas EL. Influence of particle shape on engineering properties of assemblies of two-dimensioanl polygon-shaped particles. Géotechnique 2002;57:209–17.
[44] Mitchell JK. Fundamentals of soil behaviour. New York: Wiley; 1976.
[45] Bardet JP, Huang Q. Rotational stiffness of cylindrical particle contacts. In: Thornton C, editor. Powders & grains 93. Rotterdam: Balkema; 1993. p. 39–43.
[46] Zhou YC, Wright BD, Yang RY, Xu BH, Yu AB. Rolling friction in the dynamic simulation of sandpile formation. Physica A 1999;269:536–53.
[47] Sakaguchi H, Ozaki E, Igarashi T. Plugging of the flow of granular materials during the discharge from a silo. Int J Mod Phys B 1993;7:1949–63.
[48] Iwashita K, Oda M. Rolling resistance at contacts in simulation of shear band development by DEM. ASCE J Eng Mech 1998;124:285–92.
[49] Iwashita K, Oda M. Micro-deformation mechanism of shear banding process based on modified distinct element. Powder Technol 2000;109:192–205.
[50] Oda M, Iwashita K. Study on couple stress and shear band development in granular media based on numerical analyses. Int J Eng Sci 2000;38:1713–40.
[51] Kuhn MR, Bagi K. Particle rolling and its effects in granular materials. In: Bagi K, editor. Quasi-static deformations of particulate materials. Proceedings of the QuaDPM'03 workshop, Budapest, Hungary; 2003. p. 151–8.
[52] Kuhn MR, Bagi K. Alternative definition of particle rolling in a granular assembly. ASCE J Eng Mech 2004;130:826–35.
[53] Khan AS, Huang SJ. Continuum theory of plasticity. New York: Wiley; 1995.
[54] Jiang MJ, Harris D, Yu HS. Kinematic models for non-coaxial granular materials: Part I: theories. Int J Numer Anal Meth Geomech 2005;29(7):643–61.
[55] Bardet JP, Vardoulakis I. The asymmetry of stress in granular media. Int J Solids Struct 2001;38(2):353–-367.
[56] McDowell GR, Harireche O. Discrete element modelling of soil particle fracture. Géotechnique 2002;52:131–5.
[57] Shen ZJ. Theoretical soil mechanics. Beijing: China Hydro-electric Press; 2000 [in Chinese].
[58] Jiang MJ, Konrad JM, Leroueil S. An efficient technique for generating homogeneous specimens for DEM studies. Comput Geotech 2003;30(7):579–97.
[59] Jiang MJ, Leroueil S, Konrad JM. Insight into shear strength functions of unsaturated granulates by DEM analyses. Comput Geotech 2004;31(6):473–89.
[60] Masson S, Martinez J. Micromechanical analysis of the shear behaviour of a granular material. ASCE J Eng Mech 2001;127(10):1007–16.
[61] Tordesillas A, Walsh SDC. Incorporating rolling resistance and contact anisotropy in micromechanical models of granular media. Powder Technol 2002;124:106–11.
[62] Kruyt NP. Statics and kinemtics of discrete Cosserat-type granular materials. Int J Solids Struct 2003;40(3):511–34.
[63] Delenne JY, Youssoufi MSE, Cherblanc F, Benet JC. Mechanical behaviour and failure of cohesive granular materials. Int J Numer Anal Methods Geomech 2004;28(15):1577–94.
[64] Monteiro-Azevedo N, Lemos JV. A generalized rigid particle contact model for fracture analysis. Int J Numer Anal Meth Geomech 2005;29(15):269–85.